NONLINEAR AEROELASTIC SIGNAL ANALYSIS OF AN AIRFOIL-AILERON COMBINATION

Hekmat Alighanbari
Ryerson University, Toronto, Canada

Keywords: *Aeroelasticity, Flutter, Nonlinear Dynamics*

Abstract

An airfoil-aileron combination is modeled as a three-degree-of-freedom system oscillating in plunge, pitch and aileron angular deflection, and subject to incompressible flow. The aeroelastic behaviour of the system is investigated taking into account freeplay nonlinearities in the pitch and aileron restoring moments of the airfoil. Then, the time series of the nonlinear system response are analyzed using the nonlinear dynamics methodology of parameters identification. The estimated parameters obtained via the signal processing technique are then compared with those directly calculated from the model. In the signal processing technique, first the phase–space is reconstructed using the mutual information function and the percentage of false neighbours methods. The dynamics of the system is then determined from the Lyapunov exponents. This paper discusses the limit cycle oscillations and chaotic behaviour of the 3-DOF aeroelastic system, and the tools to analyze these phenomena.

1 Introduction

Aeroelastic phenomena are a potential source of instability problems for aircraft wings. One of the most important aspects of these phenomena is self-excited divergent oscillation of wings known as flutter. This catastrophic phenomenon occurs at speeds above a critical value called flutter speed. The onset of flutter can be predicted by analyzing the flight test data acquired at speeds below the critical flutter speed.

Various methods are being used by airframe manufacturers for flutter investigation and the estimation of flutter speed. Most of these methods are typically based on the assumption of linearity, and usually work very well for linear systems. However, there are several potential sources of nonlinear behaviour on modern aircraft, and prediction of flutter speed using the linear theories may not be adequate in these cases.

The objective of this investigation is to explore the behaviour of an airfoil-aileron combination with freeplay structural nonlinearities in the pitch and aileron restoring moments, and to use modern nonlinear dynamics methodologies for the identification of flutter parameters from recorded time series. This method is expected to give a better prediction for the dynamics of the nonlinear systems.

2 Aeroelastic Equations of Motion

The equations of motion for the two-dimensional airfoil-aileron combination shown schematically in Figure 1(a) may be written in nondimensional form as

$$x''(t) + x_a a''(t) + x_b b''(t) + 2z_x \frac{\overline{w}_x}{U^*} x'(t)$$

$$+ \left(\frac{\overline{w}_x}{U} \right)^2 x = p(t, x, a, b), \tag{1}$$

$$\frac{x_a}{r_a^2} x''(t) + a''(t) + \frac{z_b}{r_a^2} b''(t) + 2z_a \frac{1}{U} a'(t)$$

$$+ \frac{1}{U^2} M(a) = r(t, x, a, b), \tag{2}$$

$$\frac{x_b}{r_b^2}\boldsymbol{x}''(\boldsymbol{t}) + \frac{z_b}{r_b^2}\boldsymbol{a}'(\boldsymbol{t}) + \boldsymbol{b}''(\boldsymbol{t}) + 2z_b\frac{\overline{w}_b}{U}\boldsymbol{b}'(\boldsymbol{t})$$

$$+ \left(\frac{\overline{w}_b}{U}\right)^2 H(\boldsymbol{b}) = w(\boldsymbol{t},\boldsymbol{x},\boldsymbol{a},\boldsymbol{b}), \tag{3}$$

where $\boldsymbol{x} = h/b$ is the nondimensional heave displacement; $(\ )'$ denotes differentiation with respect to nondimensional time $\boldsymbol{t} = tV/b$; $M(\boldsymbol{a})$ and $H(\boldsymbol{b})$ are nonlinear functions representing the restoring moments in pitch and aileron, respectively, normalized with respect to the linear stiffnesses; p, r and w are the nondimensional aerodynamic force and moments defined as

$$p(\boldsymbol{t}) = \frac{-L}{mV^2/b}, \qquad r(\boldsymbol{t}) = \frac{-M_a}{mV^2 r_a^2},$$

$$w(\boldsymbol{t}) = \frac{-M_b}{mV^2 r_b^2};$$

U is nondimensional airspeed; r_a is the nondimensional airfoil radius of gyration about the elastic axis, r_b is the nondimensional aileron radius of gyration about the aileron hinge line, and $z_b = r_b^2 + (c_b - a_h)x_b$; and, z_x, z_a and z_b are viscous damping ratios in plunge, pitch and aileron, respectively. $\overline{w}_x$ and $\overline{w}_b$ are uncoupled frequency ratios defined as

$$\overline{w}_x = \sqrt{\frac{K_x/m}{K_a/I_a}} \quad \text{and} \quad \overline{w}_b = \sqrt{\frac{K_b/m}{K_a/I_a}},$$

where m is the mass of airfoil-aileron, I_a the mass moment of inertia of the airfoil-aileron about the elastic axis, I_b the mass moment of inertia of the aileron about the aileron hinge; and, K_ξ , K_a and K_b are linearized stiffnesses in plunge, pitch and aileron hinge, respectively.

Due to the possibility of non-periodic motions of the airfoil, Theodorsen's equations cannot be employed in the present analysis. Thus, the aerodynamic force and moments are derived for any arbitrary motion of the airfoil-aileron from Theodorsen's equations by means of a Fourier analysis[1], giving

$$L(\boldsymbol{t}) = \boldsymbol{p}rbV^2\left[\boldsymbol{x}''(\boldsymbol{t}) - a_h\boldsymbol{a}''(\boldsymbol{t}) - \frac{T_1}{\boldsymbol{p}}\boldsymbol{b}''(\boldsymbol{t}) + \boldsymbol{a}'(\boldsymbol{t}) - \frac{T_4}{\boldsymbol{p}}\boldsymbol{b}'(\boldsymbol{t}) + 2(XTM)\right] \tag{4}$$

$$M_a(\boldsymbol{t}) = \boldsymbol{p}rb^2V^2\left\{a_h\boldsymbol{x}''(\boldsymbol{t}) - (\tfrac{1}{8}+a_h^2)\boldsymbol{a}''(\boldsymbol{t})\right.$$

$$+ \tfrac{1}{\boldsymbol{p}}[T_7 + (c_b - a_h)T_1]\boldsymbol{b}''(\boldsymbol{t}) - (\tfrac{1}{2}-a_h)\boldsymbol{a}'(\boldsymbol{t})$$

$$- \tfrac{1}{\boldsymbol{p}}[T_1 - T_8 - (c_b - a_h)T_4 + T_{11}/2]\boldsymbol{b}'(\boldsymbol{t})$$

$$\left. - \tfrac{1}{\boldsymbol{p}}(T_4 + T_{10})\boldsymbol{b}(\boldsymbol{t}) + 2(\tfrac{1}{2}+a_h)(XTM)\right\} \tag{5}$$

$$M_b(\boldsymbol{t}) = \boldsymbol{p}rb^2V^2\left\{\tfrac{T_1}{\boldsymbol{p}}\boldsymbol{x}''(\boldsymbol{t}) + \tfrac{1}{\boldsymbol{p}}[T_7\right.$$

$$+ (c_b - a_h)T_1]\boldsymbol{a}''(\boldsymbol{t}) + \tfrac{T_3}{\boldsymbol{p}^2}\boldsymbol{b}''(\boldsymbol{t})$$

$$+ \tfrac{1}{\boldsymbol{p}}[\tfrac{1}{3}\left(1-c_b^2\right)^{3/2} + T_1 + T_4/2]\boldsymbol{a}'(\boldsymbol{t})$$

$$\left. + \tfrac{T_4T_{11}}{2\boldsymbol{p}^2}\boldsymbol{b}'(\boldsymbol{t}) + \tfrac{T_4T_{10}+T_5}{\boldsymbol{p}^2}\boldsymbol{b}(\boldsymbol{t}) - \tfrac{T_{12}}{\boldsymbol{p}}(XTM)\right\} \tag{6}$$

where

$$(XTM) = \boldsymbol{f}(\boldsymbol{t})\left[\boldsymbol{x}'(0) + (\tfrac{1}{2}-a_h)\boldsymbol{a}'(0)\right.$$

$$+ \tfrac{T_{11}}{2\boldsymbol{p}}\boldsymbol{b}'(0) + \boldsymbol{a}(0) + \tfrac{T_{10}}{\boldsymbol{p}}\boldsymbol{b}(0)\right]$$

$$+ \int_0^{\boldsymbol{t}}\boldsymbol{f}(\boldsymbol{t}-\boldsymbol{s})\left[\boldsymbol{x}''(\boldsymbol{s}) + (\tfrac{1}{2}-a_h)\boldsymbol{a}''(\boldsymbol{s})\right.$$

$$\left. + \tfrac{T_{11}}{2\boldsymbol{p}}\boldsymbol{b}''(\boldsymbol{s}) + \boldsymbol{a}'(\boldsymbol{s}) + \tfrac{T_{10}}{\boldsymbol{p}}\boldsymbol{b}'(\boldsymbol{s})\right]d\boldsymbol{s}$$

Figures 1(b) and 1(c) show the nonlinearities assumed for the pitch and aileron moments. The nonlinear moment $M(\boldsymbol{a})$ and $H(\boldsymbol{b})$ are given by

$$M(\boldsymbol{a}) = \begin{cases} \boldsymbol{a} - \boldsymbol{a}_f + M_0 & \text{for } \boldsymbol{a} < \boldsymbol{a}_f, \\ M_0, & \text{for } \boldsymbol{a}_f \le \boldsymbol{a} \le \boldsymbol{a}_f + d, \\ \boldsymbol{a} - \boldsymbol{a}_f - d + M_0, & \text{for } \boldsymbol{a} + d < \boldsymbol{a}, \end{cases}$$

$$H(\boldsymbol{b}) = \begin{cases} \boldsymbol{b} - \boldsymbol{b}_f + H_0 & \text{for } \boldsymbol{b} < \boldsymbol{b}_f, \\ H_0, & \text{for } \boldsymbol{b}_f \le \boldsymbol{b} \le \boldsymbol{b}_f + d_b, \\ \boldsymbol{b} - \boldsymbol{b}_f - d_b + H_0 & \text{for } \boldsymbol{b} + d_b < \boldsymbol{b}., \end{cases}$$

3 Nonlinear Signal Processing

Aeroelastic investigation of airfoils with structural nonlinearities has shown that for velocities below the linear flutter boundary the airfoil can be stable or it can oscillate indefinitely in a periodic or chaotic manner.

In such cases, the usual flutter parameter identification tools based on linear signal processing techniques may not be adequate.

Thus, one needs to have some reliable means to analyze nonlinear response signals having decaying, periodic or chaotic characteristics. There are various suggested approaches on this subject, and amongst these methods, an approach used by nonlinear dynamicists offers a great potential in flutter signal analysis [2].

The proposed signal processing technique consists of the following steps.

1- Signal measurement
2- Signal separation
3- Phase-space reconstruction
4- Estimation of system invariants
5- Model making and predictions

The time series of the response can be obtained experimentally by placing sensors such as accelerometers or strain gages on the aircraft structure. The signals are digitally sampled, and they are scalar quantities designated by $x(n)$ where n is the sample number which can be converted to time once the sampling frequency is given.

For nonlinear systems with possibly chaotic oscillations, one would like to separate noise from the signal without influencing the possibly chaotic behaviour of the signal. The signal separation process favoured by nonlinear dynamicists is the manifold decomposition method[2].

3.1 Phase-Space reconstruction

After the signal preparation, a phase-space reconstruction is carried out using time-delay method. To construct the phase-space one would typically need to obtain all variables of the system, positions and velocities. However, one really does not need all these to capture the structure of the orbit. For the purpose of creating a phase-space any smooth nonlinear change of variables will act as a coordinate basis for the dynamics. Starting from the observed scalar quantity $x(n)$, the state space vector $y(n)$ could be formed in d_e-dimensional space using a time-delay T,

$$y(n) = [x(n), x(n+T), x(n+2T) \ldots$$
$$\ldots x(n+(d_e-1)T)] \tag{7}$$

Plotting this vector in a d_e dimensional space represents the phase-space of the system.

The key point in the time-delay reconstruction method is that $x(n)$ and $x(n+T)$ are related by the evolution of the dynamical system over a period of time T during which all dynamical variables affect the observed variable $x(n)$. Therefore, $x(n+T)$ is an unknown, nonlinear combination of all variables of the system. Alone, it may represent one of the variables, but the combination into a d_e-dimensional vector of time-delays of $x(n)$ represents d_e active variables of the system being observed.

Selection of appropriate time-delay T, is important in the reconstruction technique. If the time-delay is too short, not enough time will elapse for the system to produce information about its dynamics. If it is too large, too much information will be lost, and the two data samples will not be correlated. The optimum time-delay can be obtained using the average mutual information function[3][5]. The average mutual information identifies how much information one can learn about a measurement at one time, $x(n+T)$, from a measurement taken at another time, $x(n)$. The expression for the mutual information is given by

$$I(T) = \sum_{n=1}^{N} P[x(n), x(n+T)]$$
$$\log_2 \left[\frac{P[x(n), x(n+T)]}{P[x(n)].P[x(n+T)]} \right] \tag{8}$$

where $P[x(n)]$ and $P[x(n+T)]$ are, respectively, the probabilities of $x(n)$ and $x(n+T)$ occurring in the data set, and $P[x(n), x(n+T)]$ is the joint probability. N is the total number of observed variable $x(n)$. The value of time-delay T at which the first minimum of the mutual information occurs is then judged as the appropriate time-delay to be used in the phase-space reconstruction technique. If the average mutual information has no minimum, it is recommended[2] to use T such that $I(T)/I(0) \cong 1/5$. By selecting T using the above methods, the values of $x(n)$ and $x(n+T)$ are

independent enough of each other to be useful as coordinates in time delay vector but not so independent as to have no connection with each other at all.

To reconstruct the phase-space one also needs to determine the dimension of the phase-space or so called "embedding dimension". To find the embedding dimension d_e, the method of false nearest neighbours is used in the present analysis[5][6]. In this method, first the state space is reconstructed in a dimension d_e, and the Euclidian distances between each point and its nearest neighbouring points in the reconstructed state space are calculated. The distance between point $y(n)$ and its rth nearest neighbour, $y^r(n)$, is calculated from

$$R_{de}^2(n,r) = \sum_{k=0}^{de-1} [x(n+kT) - x^r(n+kT)]^2 \qquad (9)$$

for $r = 1, 2, \ldots, N_b$. Then, the process is repeated in a space dimension d_e+1,

$$R_{de+1}^2(n,r) = R_{de}^2(n,r) + [x(n+d_eT) \\ - x^r(n+d_eT)]^2 \qquad (10)$$

If $y^r(n)$ is a true neighbour, then it arrives at the neighbourhood of $y(n)$ in the state space through dynamic origins. It is a false neighbour if it arrives in the neighbourhood of $y(n)$ because the present dimension did not fully unfold the attractor, and by increasing the embedding dimension to d_e+1, it is possible to move $y^r(n)$ out of the neighbourhood of $y(n)$. The $y(n)$ and $y^r(n)$ are considered neighbours if the distance between them stays within a tolerance R_{tol} when the embedding dimension is increased from d_e to d_e+1. The criterion for designating a neighbour to be false is given by Kennel et al.[6] as follows:

$$\left[\frac{R_{de+1}^2(n,r) - R_{de}^2(n,r)}{R_{de}^2(n,r)} \right]^{1/2} \\ = \frac{\left| x(n+d_eT) - x^r(n+d_eT) \right|}{R_{de}(n,r)} > R_{tol} \qquad (11)$$

Kennel et al.[6] suggest $R_{tol} > 10$. Once the percentage of false neighbours falls below some specified limit, then, the corresponding dimension may be chosen as a sufficient

embedding dimension. Kennel et al.[6] suggest the limit to be 1%.

Figure 2 is presented here to show few concepts of the phase-space reconstruction. Consider a set of available data, $x(n)$. Figure 2 shows the reconstructed phase-space in a 2-D space, $d_e = 2$. Definition of nearest neighbours is presented by showing, for example, the 1st neighbour of a typical point $y(n)$. Two points A and B in the crossing point seem to be very close neighbours in the 2-D space. However, these points are false neighbours, and reconstructing the phase-space in 3-D separates the two points and the distance between them increases significantly.

3.2 Calculation of System Invariants

After reconstructing the phase-space, one should be able to classify the dynamical system by finding the invariants of the system. Eigenvalues are the invariants for a linearized system. For a nonlinear system Lyapunov exponents are the most important invariants. To determine the exponents, one may use the evolution of the state space vector given by[7][8][9]

$$y(n+T) = F(y(n)) \qquad (12)$$

This is the governing map for the reconstructed orbit. Function F is not known in algebraic form, but locally it can be estimated from the reconstructed space. At each point on the orbit $y(n)$, a Taylor series for $F(y(n))$ is made in the vicinity of the orbit, and the Taylor coefficients are determined numerically by a least square fit to the data.

Small perturbations to the orbit evolve according to the linearized dynamics

$$\Delta y(n+T) = DF(n)\Delta y(n) \qquad (13)$$

where $DF(n)$ is the Jacobian matrix of the map $F(n)$ at location $y(n)$ on the orbit. The Jacobian matrices can be approximated from the linear term of the calculated Taylor series for $F(y(n))$. Once the Jacobian matrix of the mapping $F(y(n))$ for each point in the state space is known, one can use the Multiplicative Eergodic Theorem of Oseledec to determine the Lyapunov exponents of the system[10]. The theorem states that if we form Oseledec matrix

$$OSL(n, L) = \left(\left(DF^L(n) \right)^T . DF^L(n) \right)^{\frac{1}{2L}} \qquad (14)$$

then the limit of this as $L \rightarrow \infty$ exists, and it is independent of $y(n)$. Lyapunov exponents are simply the logarithm of the eigenvalues of this matrix when $L \rightarrow \infty$. $DF^L(n)$ is the product of L Jacobians matrices,

$$DF^L(n) = DF(n) . DF(n-1) \ldots DF(1),$$

where dots represent matrix multiplication. Details of the above procedure can be found in the paper by Brown et al.[9].

After calculating the Jacobian matrix, one may adapt the following methodology to calculate the linearized modal damping and frequencies of the system. Using an exponential representation, one can write a space perturbation $\boldsymbol{D}y$ which will evolve according to the expression

$$\Delta y(n + T) = \exp \left([A] T \Delta t \right) \Delta y(n) \qquad (15)$$

where the matrix $[A]$ determines the system dynamics. Comparing Equation (15) with Equation (13) gives the following:

$$\exp \left([A] T \Delta t \right) = DF(n) \qquad (16)$$

The Jacobian matrix depends on location in the phase-space and hence the term $\exp \left([A] T \Delta t \right)$ obtained numerically will not be constant for every state vector in the phase-space. However, they can be averaged to obtain a mean $\exp \left([A] T \Delta t \right)$ matrix, and the average complex exponents $\boldsymbol{I}_{1cplx}$, $\boldsymbol{I}_{2cplx} \ldots \boldsymbol{I}_{decplx}$. These exponents are the eigenvalues of logarithm of the averaged matrix divided by $T\boldsymbol{D}t$. Knowing the complex exponents, the frequency and damping values of the system can be obtained from the following expressions:

$$\boldsymbol{z}_i = \frac{\mathrm{Re} \left(\boldsymbol{I}_{icplx} \right)}{\sqrt{\left[\mathrm{Re} \left(\boldsymbol{I}_{icplx} \right) \right]^2 + \left[\mathrm{Im} \left(\boldsymbol{I}_{icplx} \right) \right]^2}} \qquad \textbf{(17)}$$

$$\boldsymbol{w}_i = \frac{\mathrm{Re} \left(\boldsymbol{I}_{icplx} \right)}{2 \boldsymbol{p} \boldsymbol{z}_i} \qquad \textbf{(18)}$$

3.3 Model Making and Predictions

Finding instability points, such as flutter speed, is desirable in the analysis of aeroelastic

system. For prediction of such points, first, behaviour of the system at airspeeds below the critical speed should be analyzed and the attractors of the system and their corresponding invariants should be identified. Then, the following methods could be used to predict the system behaviour at higher speeds.

First method is based on the understanding of the fundamental physics of the problem. In this method, one develops a set of governing equations for the aeroelastic system and then compares the output of those equations to properties of the reconstructed state space. The comparison is to be made in terms of the quantities such as Lyapunov exponents. The characteristic parameters of the equations could be adjusted based on the comparisons. The refined model then can be used to predict the system behaviour at higher speeds.

Second method is to extrapolate system invariants and to predict possibility of a bifurcation point at higher airspeeds. For example, assume that the system is stable at evaluated speeds. This means the system has a stable fixed-point attractor. In this case, eigenvalues of the linearized system are estimated at these speeds, and they are extrapolated to predict stability of the attractor at higher speeds. This is same as extrapolation of frequency and damping values for calculation of linear flutter speed. For an LCO solution, which represents a stable periodic attractor, Floquet multipliers are representative of the attractor's stability. Thus, in this case Floquet multipliers should be calculated for velocities below the critical speed and then extrapolated to predict stability of the solutions at higher speeds. Amplitude of the LCOs should also be extrapolated. In using this method one should bare in mind the complexity of dynamics of nonlinear aeroelastic systems. It has been shown that for such systems more than one stable solution and variety of bifurcations may exist below the linear flutter speed[1][11]. Stability of all possible solutions must be investigated in such cases.

4 Results

Flutter analysis of the airfoil-aileron combination, containing freeplay nonlinearities, shows a wide region of limit cycle oscillations for airspeeds below the linear flutter speed. For the cases where the aileron centre of gravity is aft the aileron hinge moment, chaotic oscillations are detected at a considerable range of airspeeds.

The results presented here are for the following airfoil, aileron and nonlinearity parameters; $\overline{w}_x = 0.2$, $\overline{w}_b = 1.5$, $m = 100$, $a_h = -0.5$, $x_a = 0.25$, $r_a = 0.5$, $x_b = 0.002$, $r_b^2 = 0.002$, $M_0 = 0$, $a_f = -0.25^o$, $\delta_\alpha = 0.5^o$, $H_0 = 0$, $b_f = -0.5^o$ and $\delta_\beta = 1^o$. For this airfoil, the linear flutter speed is found to be $U^* = 6.16$.

Figure 3a is a typical bifurcation diagram of the pitch response obtained using Houbolt's finite difference method. The figure shows the value of α when $\alpha\dot{c} = 0$ (i.e. extremums of the steady-state oscillations). The significance of such a diagram is as follows: if at a particular U/U^* the system is stable, then a single point is obtained; if the motion is an LCO with one frequency, then two points are obtained, e.g. $U/U^*>0.74$; and, an LCO with two frequencies results in four points, e.g. $0.57<U/U^*<0.74$; etc. A large number of points at some velocities indicates aperiodic or possibly chaotic motion, e.g. $0.3<U/U^*<0.5$. Figure 3b shows the bifurcation diagram of the aileron motion of the same airfoil. Both bifurcation diagrams illustrate possibility of chaotic motion for a wide range of airspeed.

If freeplay nonlinearities are considered in both pitch and aileron restoring moments, then, stronger chaos in wider range of airspeed is obtained. Figure 4a and 4b show the bifurcation diagrams for this double root nonlinearity case.

Figures 5a and 6a show a sample steady-state oscillation of the airfoil in pitch and aileron directions. Phase-plane plots of the pitch and aileron motion are also presented in Figures 5b and 6b. Further analysis of the airfoil motion in terms of the Power Spectral Densities (PSD), Poincaré sections and Lyapunov exponents shows that the system behaviour is chaotic in this range of airspeed. Samples of pitch and aileron PSDs are presented in Figure 7.

The time history of the airfoil motion bears some resemblance to linear system signals corrupted with noise. Without recognizing the chaotic behaviour of the signal, one may inadvertently use linear signal processing techniques to calculate the frequency and damping values of the flutter modes from the recorded time series. This can lead to misleading results. In order to describe the system behaviour properly, we use the more suitable method, explained in the preceding section, to extract system parameters from the recorded signals.

Using the nonlinear signal processing technique described above, the phase-space can be constructed from measurements of a or b alone. The time-delay required for phase-space reconstruction is obtained using the mutual information method. The mutual information $I(T)$ for b motion is determined from Equation(8) and its variation with time-delay is shown in Figure 8. The figure shows that for small time delays $T < 3$, the mutual information is rather high. That is, reconstructed phase-space with such time delays will not be fully unfolded because the coordinates $x(n)$ and $x(n+T)$ are too much related to each other. In other word, not enough time elapsed between $x(n)$ and $x(n+T)$ that the systems dynamics fully affect $x(n+T)$. On the other hand, time delay should not be so long that $x(n)$ and $x(n+T)$ become unrelated. The best time-delay in this case for phase-space reconstruction is $T = 5$ at which the first minimum of the $I(T)$ occurs. This time-delay is then used in the false neighbours method to estimate the minimum required embedding dimension. The variation of percentage of false neighbours is presented in Figure 9 as a function of embedding dimension. Based on this, embedding dimension of 4 or higher is required to unfold this attractor.

Figures 10 and 11 show the reconstructed phase plane of the chaotic attractor. Compared with Figure 5b and 6b, which show the direct results of the simulation, it is clear that the basic structure of the chaotic attractor have been

captured. It should be noticed that the presented phase planes are two-dimensional sections from six dimensional phase-spaces.

Using the analysis given above, the Lyapunov exponents are also computed. The largest exponent is approximately 0.1 for this case. The agreement between the Lyapunov exponents obtained directly using the equations of motion and those obtained from the reconstructed phase-space is reasonably good for the largest exponent, which is the one that indicates whether or not the system is chaotic.

5 Conclusions

A 3-DOF airfoil with structural nonlinearities in pitch and aileron restoring moments exhibits rich dynamics below the linear flutter speed. A random-like response known as chaos can take place in a wide range of airspeed for this system. The time series of such signals bear some resemblance to linear system signals corrupted with noise. Without recognizing the chaotic behaviour of the signals, one may inadvertently use linear signal processing techniques to calculate the frequency and damping values of the flutter modes. Even though most available linear signal processing techniques work very well for linear systems, they can lead to misleading results for nonlinear systems. More suitable methods based on tools developed for nonlinear dynamic systems can be used to extract parameters in order to describe the system behaviour properly. The application of these techniques to aeroelasticity is still in its infancy stage. The method outlined in this paper is potentially useful to analyse nonlinear aeroelastic signals, but further studies are necessary to address the issues of noise, selection and optimization of the various parameters used in the method.

References

[1] Alighanbari, H. Aeroelastic response of an Airfoil-Aileron Combination with Structural nonlinearities. *Proceedings of Third International Conference on Nonlinear Problems in Aviation,* Daytona Beach, Florida, USA, pp. 21-30, 2000.

[2] Abarbanel, HDI. *Analysis of observed chaotic data.* Springer-Verlag, New York, 1996.

[3] Gallager, RG. *Information theory and reliable communication*. Wiley, New York 1968.

[4] Abarbanel, HDI, Brown, R, Sidorowich, JJ and Tsimring, LS. The analysis of observed chaotic data in physical systems. *Reviews of Modern Physics*, Vol. 65, pp. 1331-1392, 1993.

[5] Fraser, AM and Swinney, HL. Independent coordinates for strange attractors from mutual information. *Physical Review A*, Vol. 33, pp. 1134-1140, 1986.

[6] Kennel, MB, Brown, R and Abarbanel, HDI. Determining embedding dimension for phase-space reconstruction using geometrical construction. *Physical Review A*, Vol. 45, pp. 3403-3411, 1992.

[7] Briggs, K. An improved method for estimating Lyapunov exponents of chaotic time series. *Physical Letters A*, Vol. 151, pp. 27-32, 1990.

[8] Bryant, P, Brown, R and Abarbanel, HDI. Lyapunov exponents from observed time series. *Physical Review Letters.* Vol. 65, pp. 1523-1526, 1990.

[9] Brown, R, Bryant, P and Abarbanel, HDI. Computing the Lyapunov spectrum of a dynamical system from an observed time series. *Physical Review A*, Vol. 43, pp. 2787-2806, 1991.

[10] Oseledec, V. A multiplicative ergodic theorem. Lyapunov characteristic numbers for dynamical systems. *Trans. Moscow Math. Soc.* Vol. 19 , pp. 197-231, 1968.

[11] Alighanbari, H and Price, SJ. The Post-Hopf-Bifurcation Response of an Airfoil in Incompressible Two-Dimensional Flow. *Nonlinear Dynamics*, Vol. 10, pp. 381-400, 1996.
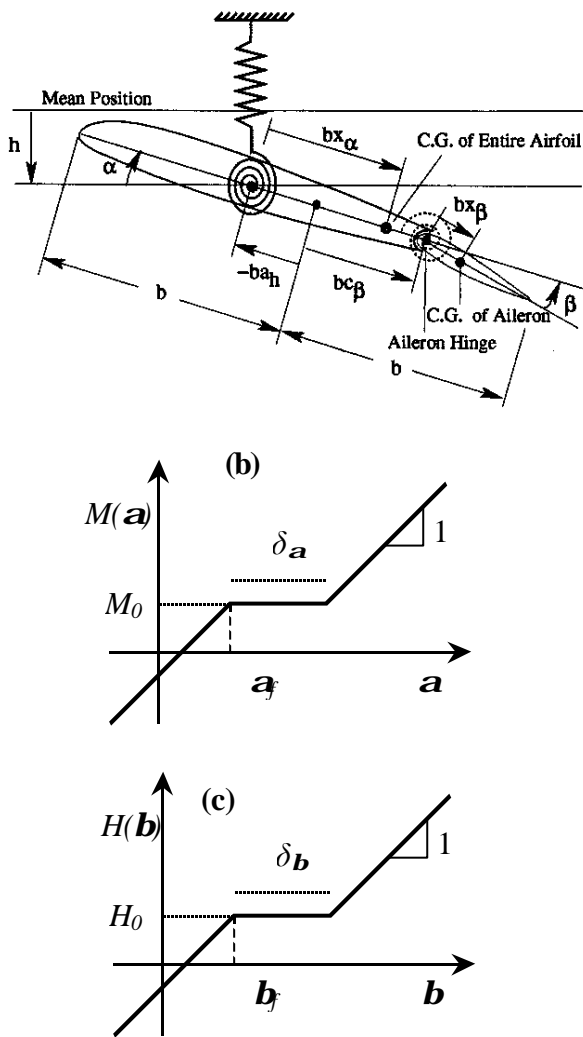
Fig.1. (a) Schematic of the three-DOF airfoil (b) freeplay in pitch moment; (c) freeplay in aileron moment
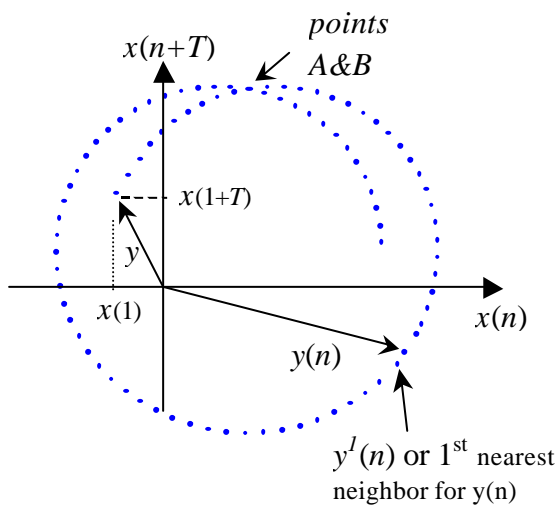
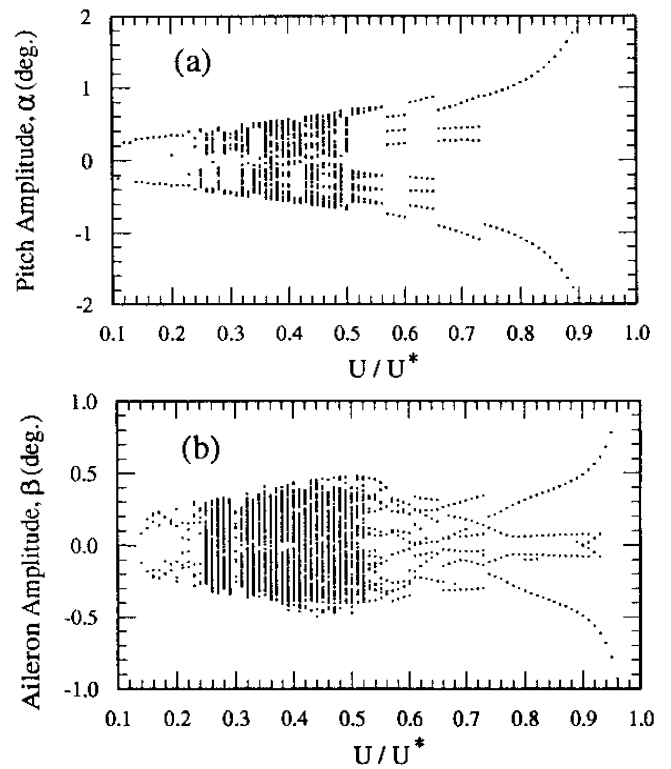

Fig.2. Schematic reconstructed phase-plane

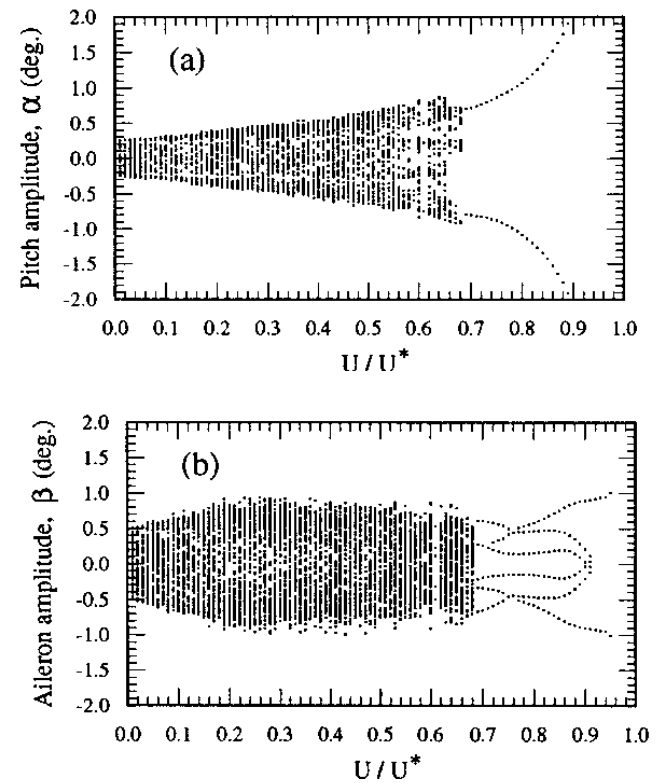Fig.3. Bifurcation diagrams for freeplay in pitch; (a) pitch angle, (b) aileron angle.

Fig.4. Bifurcation diagrams for freeplay in both pitch and aileron; (a) pitch angle, (b) aileron angle.
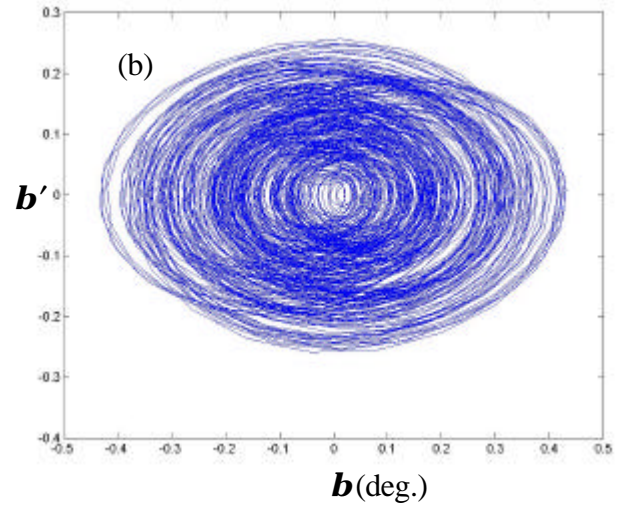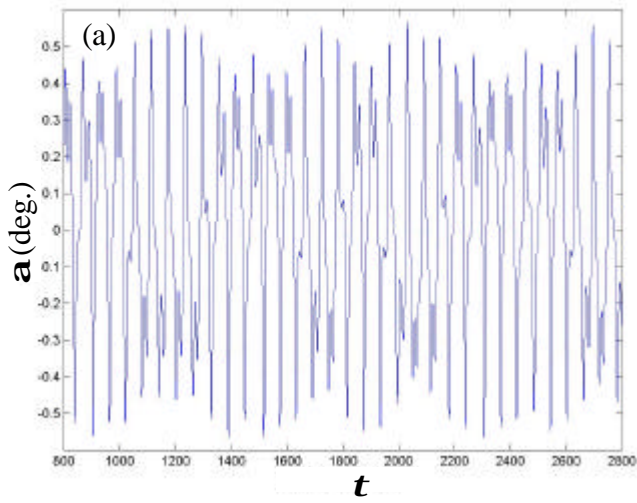
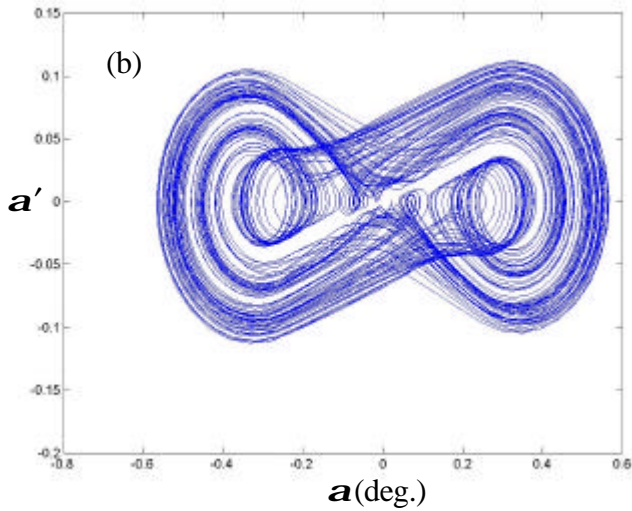Fig.5. (a) Time history of pitch angle α, (b) Phase-plane plot
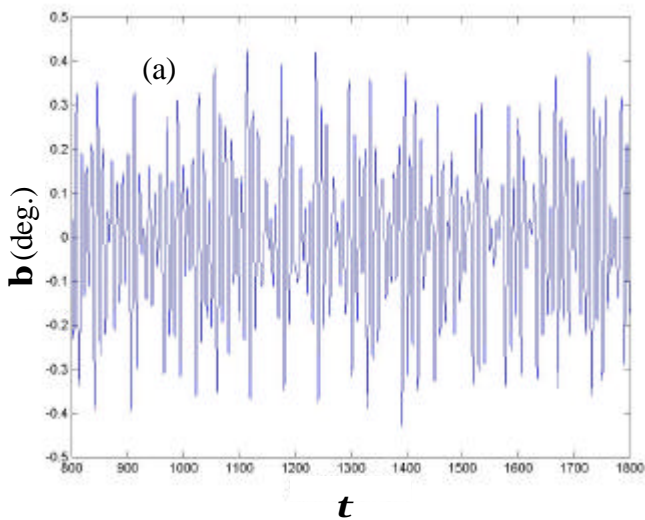

Fig.6. (a) Time history of aileron angle β, (b) Phase-plane plot
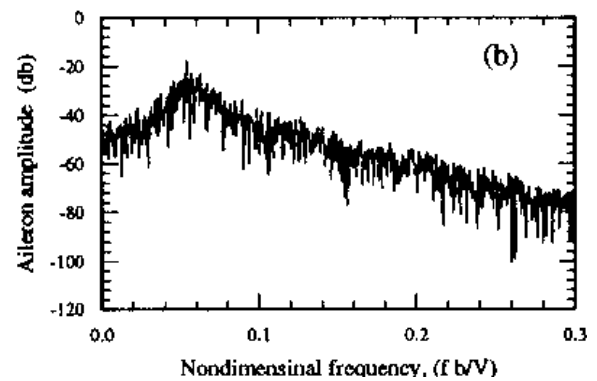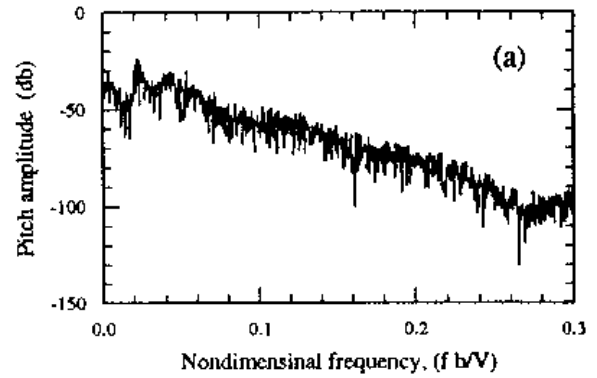
Fig.7. Sample Power Spectral Densities for the same airfoil as Figure 4.
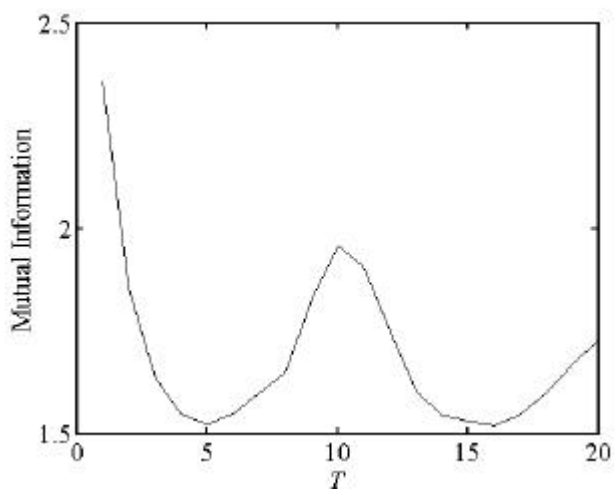
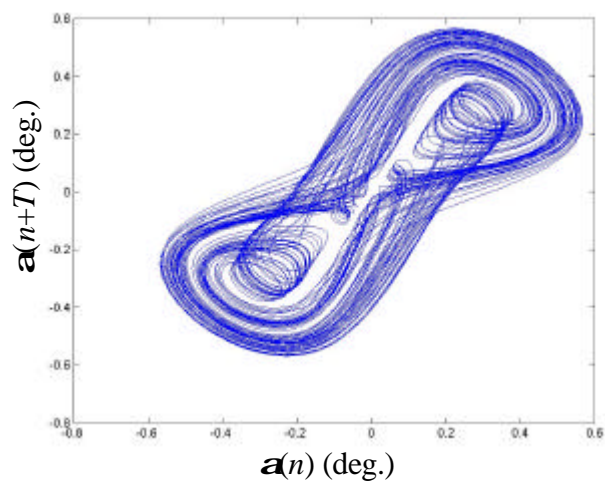Fig.8. Variation of mutual information with time-delay for the aileron response

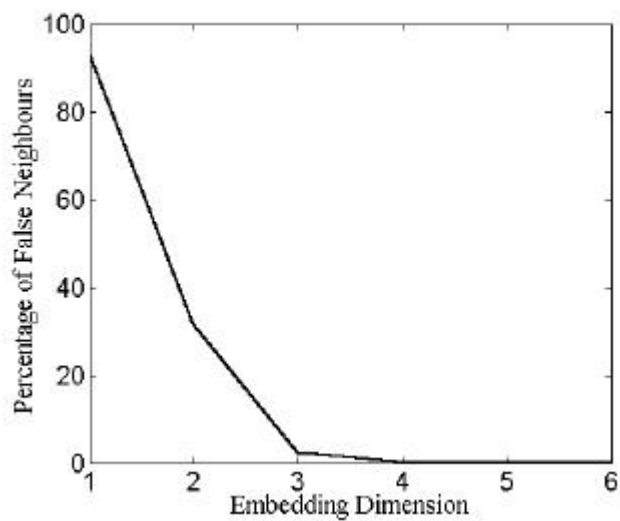Fig.10. Reconstructed phase-plane of the pitch degree of freedom

Fig.9. Variation of False Neighbors percentage with embedding dimension for the aileron response
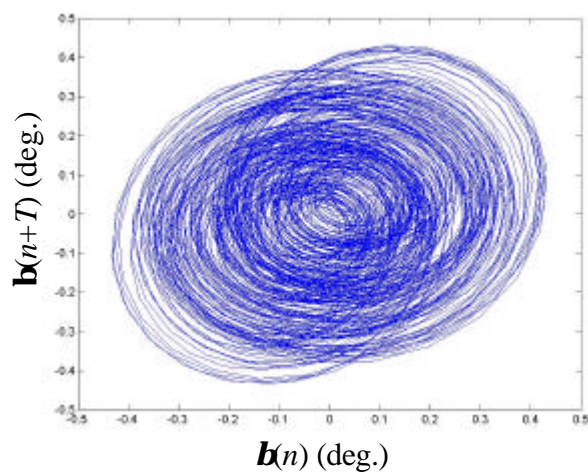

Fig.11. Reconstructed phase-plane of the aileron degree of freedom